Research Article

Jhonatan M. Silva, Fernando E. Maturi, Hernane S. Barud, Vera R.L. Constantino and Sidney J.L. Ribeiro*

New organic-inorganic hybrid composites based on cellulose nanofibers and modified Laponite

https://doi.org/10.1515/aot-2018-0030
Received May 31, 2018; accepted August 29, 2018; previously published online September 28, 2018

Abstract: The combination of cellulosic materials and clays, such as Laponite, can provide composites with superior optical and mechanical properties compared to pristine cellulose. Synthetic clays can also be used as a host matrix for the immobilization of luminescent complexes, as the incorporated complexes may present enhanced emission quantum efficiency, photo and thermostability compared to the non-immobilized ones. In this way, we, herein, report the preparation of luminescent composites through the incorporation of a Eu(III) complex $[Eu^{3+}(tta)_n]$ containing Laponite (Lap) into cellulose nanofibers (CNF). The thermogravimetry results show that the obtained CNF/Lap@$[Eu^{3+}(tta)_n]$ films present higher thermal resistance than the CNF film. The $Eu^{3+}(tta)_n$ species were found in the composite structure with preserved luminescence characteristics, and no leaching or degradation of the organic ligand was observed with the preparation of the composites.

Keywords: cellulose nanofibers; europium; Laponite; luminescent composites; luminescent films.

***Corresponding author: Sidney J.L. Ribeiro,** Institute of Chemistry, São Paulo State University (UNESP), CP355 Araraquara-SP 14800-900, Brazil, e-mail: sidney@iq.unesp.br. http://orcid.org/0000-0002-8162-6747
Jhonatan M. Silva and Fernando E. Maturi: Institute of Chemistry, São Paulo State University (UNESP), CP355 Araraquara-SP 14800-900, Brazil
Hernane S. Barud: Biotechnology Research Center, University of Araraquara (Uniara), 1338 Carlos Gomes Street, Araraquara-SP 14801-340, Brazil
Vera R.L. Constantino: Institute of Chemistry, University of São Paulo (USP), São Paulo-SP 05508-000, Brazil

1 Introduction

Laponite RD (chemical composition $Na_{0.7}[Mg_{5.5}Li_{0.3}Si_8O_{20}(OH)_4](H_2O)_n$) is a synthetic clay of the smectite family. Its structure presents 2:1 tetrahedral-octahedral-tetrahedral (TOT) layers where two sheets are formed by SiO_4 tetrahedra, and one sheet is formed by Mg^{2+} octahedral coordinated with OH groups. Compared to natural clays such as montmorillonite, Laponite presents better dispersion in aqueous systems, ability to form films and translucent gels, reduced content of transition metals (present in natural clays), and small crystallite size (diameter and thickness around 30 nm and 1 nm, respectively). These properties make Laponite a good candidate for the preparation of composites with polymeric materials, improving their physical and chemical properties [1–6].

In a unique way, synthetic Laponite stands out against natural clays due to the high transparency in aqueous systems and small crystallite size that allow its use as a host matrix for the bidimensional confinement of molecular species such as luminescent lanthanide complexes [1–5]. These 'two-dimensional shuttles' to use the term coined in [7], are, indeed, good nanometric hosts that can be used to produce new composites like the one presented in this contribution.

In general, Laponite, itself, gives rise either to powders or materials that are difficult to be processed. A good option would be to incorporate it, for example, in green support materials. Nowadays, there is a rising concern about the use of non-biodegradable plastics, and many efforts have been paid to replace petroleum-based polymers by eco-friendly alternatives. Hence, a good option would be to incorporate Laponite in natural polymers [8–10]. Among the natural polymers, cellulose nanofiber (CNF)-based materials have attracted the attention of researchers and industries as they present interesting properties, such as the ability to improve mechanical properties (tensile strength and Young's modulus) of biodegradable materials such as polylactic acid (25% and 40%, respectively) [8], epoxy composites (tensile strength 26.7 MPa) [11], low

coefficient of thermal expansion (10^{-7} K^{-1} along the longitudinal direction) [12], and good biocompatibility.

The fate of CNFs is not restricted to such applications, and there are reports of its use in the production of aerogels [13, 14], drug delivery systems [15–17], and production of composites with clays [9].

Laponite was used as a matrix for the production of luminescent hybrids [3, 4], and composites were prepared from CNFs and clays in the preparation of composites [9]. We present, here, an innovative proposal for obtaining new materials in the form of luminescent flexible films, using CNF and Laponite. The incorporation of luminescent species as Eu^{3+} complexes lead to new composites where the synergistic effect coming from CNF and Laponite counterparts added to the luminesce properties open possibilities for new photonic applications.

2 Experimental section

2.1 Materials

2-Thenoyltrifluoroacetone (htta, 99%), ethanol, and hydrochloric acid were purchased from Sigma-Aldrich and used as received. Europium(III) oxide (99.99%) was purchased from Lumintech. Laponite RD (coding S/12796/11) was provided by Buntech (Brazil). The CNFs extracted from *Eucalyptus globulus* by mechanical separation of the fibers was supplied by Suzano Paper and Cellulose Industry (Limeira-SP, Brazil). Water suspension of 2% (w/v) of cellulose was used.

2.2 Methods

2.2.1 Preparation of europium(III) containing Laponite: The procedure was adapted from literature [3, 4]. Europium(III) chloride was obtained by dissolution of 0.65 g of europium(III) oxide in 1.10 ml of hydrochloric acid. A Laponite water suspension (5% w/w) was prepared using 1.5 g of clay and 28.5 ml of ultrapure water, under mechanical stirring for 10 min and followed by sonication, also for 10 min, leading to a colorless gel. The europium(III) chloride water solution (20 ml, 1.5 mmol, pH 4.5) was added under mechanical stirring, and the mixture was kept under constant stirring at 80°C for 24 h to promote the intercalation of the Eu^{3+} ions between the Laponite layers. The product, called Lap@Eu, was collected by centrifugation, washed with ultrapure water, and dried at 80°C for 15 h. It was ground to a white powder afterward.

2.2.2 *In situ* formation of europium(III) complex into Laponite: The methodology of this step was also based on previous works [3, 4], in which the preparation of complexes of the general formula$[Eu(tta)_n]$ was achieved through the cation exchange of the Na^+ ion by Eu^{3+} and later loading tta (unprotonated form of htta). In this way, the *in situ* formation of the Lap@$[Eu(tta)_n]$ complex into the Laponite-layered structure was achieved by the addition of htta ligand to the Lap@Eu water suspension. An ethanolic htta solution (30.0 g, 10 ml) was added to an aqueous suspension of the previously prepared Lap@Eu (1.0 g, 20 ml). The resulting mixture was sonicated (270 W) at room temperature (25°C) for 2 h, filtered, washed with ethanol, and dried at 50°C overnight. The product, named Lap@$[Eu(tta)_n]$, was ground to a light-yellow powder. The general preparation procedure is depicted schematically in Figure 1.

2.2.3 Luminescent CNF/Lap@$[Eu(tta)_n]$ films: Nanocomposite films were prepared by mixing CNF and Lap@Eu(tta) hybrid water suspensions followed by drying. Films were produced by varying the CNF to hybrid dry mass ratio. Suspensions of the hybrids were prepared adding 1 ml of ultrapure water to different amounts of hybrid [0.021 and 0.042g of Lap@ Eu^{3+}(tta)]. Two milliliters of CNF aqueous suspension was added to these suspensions, corresponding to 2:1 and 1:1 CNF:Lap@Eu(tta) weight ratio. The resulting suspensions were dried in 35-mm-diameter polystyrene Petri dishes at 25°C for 5 days leading to the self-sustainable film formation.

2.2.4 Characterization: The thickness of the films was measured using a Mitutoyo (Kawasaki, Kanagawa, Japan) mechanical micrometer (0.001 mm resolution) at three distinct points in the films. Scanning electron microscopy (SEM) images and energy-dispersive X-ray spectroscopy (EDS) were carried out in a JEOL (Akishima, Tokyo, Japan) electron microscope, model JSM-7500F, with field emission gun (FEG-MEV), and an acceleration voltage of 10 kV. X-ray diffractograms were registered on a Siemens® (Munich, Germany) 246 D5000 diffractometer (tube operating at 40 kV and 30 mA), from 2° to 50° (2θ), using the Cu-Kα radiation (1.5418 Å) and 0.02° increment. A thermogravimetric analysis (TGA) was performed on a TA Instruments (New Castle, DE, USA) SDQ Q600 equipment with a 10°C min^{-1} heating rate

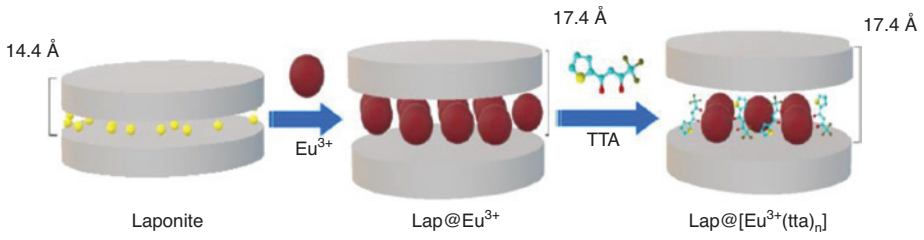

Figure 1: Schematic representation of the steps of intercalation of Laponite with the Eu^{3+} ions and the *in situ* preparation of the [Lap@$Eu(tta)_n$] hybrid.

using alumina crucibles under synthetic airflow (100 ml min^{-1}). Onset temperatures (T_{onset}) were obtained using the TA Universal Analysis software (New Castle, DE, USA). Photoluminescence measurements were performed on a Horiba Jobin Yvon (Kyoto, Japan) Fluorolog-3 FL3-122 spectrofluorimeter. Photoluminescence (PL) and photoluminescence excitation (PLE) spectra were recorded at room temperature with spectral resolution of 0.5 nm and corrected for the spectra response of the excitation and the emission setup. Emission lifetimes were obtained by monitoring the emission decay curve of Eu^{3+}, $^5D_0 \rightarrow {}^7F_2$ transition (615 nm), exciting at 340 nm. A Xe pulsed (3-µs bandwidth) lamp and the phosphorimeter Horiba accessory were used. Decay curves were fitted to an exponential function.

3 Results and discussion

Typical self-sustainable film samples are shown in Figure 2. Thickness values of 0.149 ± 0.004 µm and 0.237 ± 0.019 µm were measured for 2:1 and 1:1 CNF:hybrid weight ratio, respectively. As observed in the figure, the obtained films presents an opaque aspect, which is well explained by the presence of Lap@[Eu(tta)$_n$] aggregates.

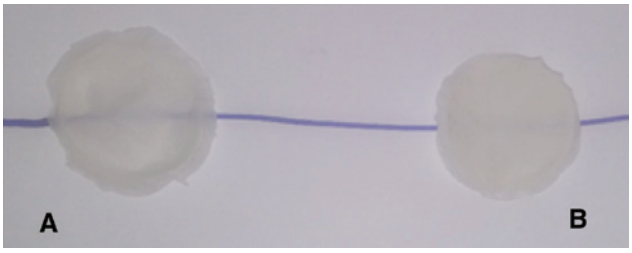

Figure 2: Film picture. CNF/[Lap@Eu(tta)$_n$] 2:1 (A) and 1:1 (B). Sample diameter ~3.5 cm.

SEM images (Figure 3A and B) show aggregates of different sizes in micrometric scale. Figure 3 also shows images for CNF/Lap@[Eu(tta)$_n$] 1:1 (surface in Figure 3C and cross-section in Figure 3E) and 2:1 (surface in Figure 3D and cross-section in Figure 3F). The surface of both 2:1 and 1:1 samples display cellulose fibers covering several aggregates of the Lap@[Eu(tta)$_n$]. Cross-section images clearly show aggregates of the hybrid among the fibers of cellulose.

The EDS measurements (Figure 4) show peaks referring to the elements magnesium (Mg) and silicon (Si), constituents of Laponite.

Figure 5 shows X-ray diffraction patterns obtained for Laponite, Lap@Eu, and Lap@[Eu(tta)$_n$] samples. The incorporation step of the Eu^{3+} ion and the successive addition of the htta ligand did not modify the Laponite-layered structure. The diffraction peaks at (2θ) 19.77°, 28.32°, and 34.96°, corresponding to the planes (110), (005), and (200) of the clay [18], can be observed in the diffractograms obtained for Lap@Eu and Lap@Eu(tta). The insertion of species between the layers (intercalation process) leads to an increase in the clay interlayer space (basal spacing or interlamellar space), which is manifested in the shift of the peak related to the (001) plane toward smaller 2Θ values. Thus, through the band d001 and using Bragg's

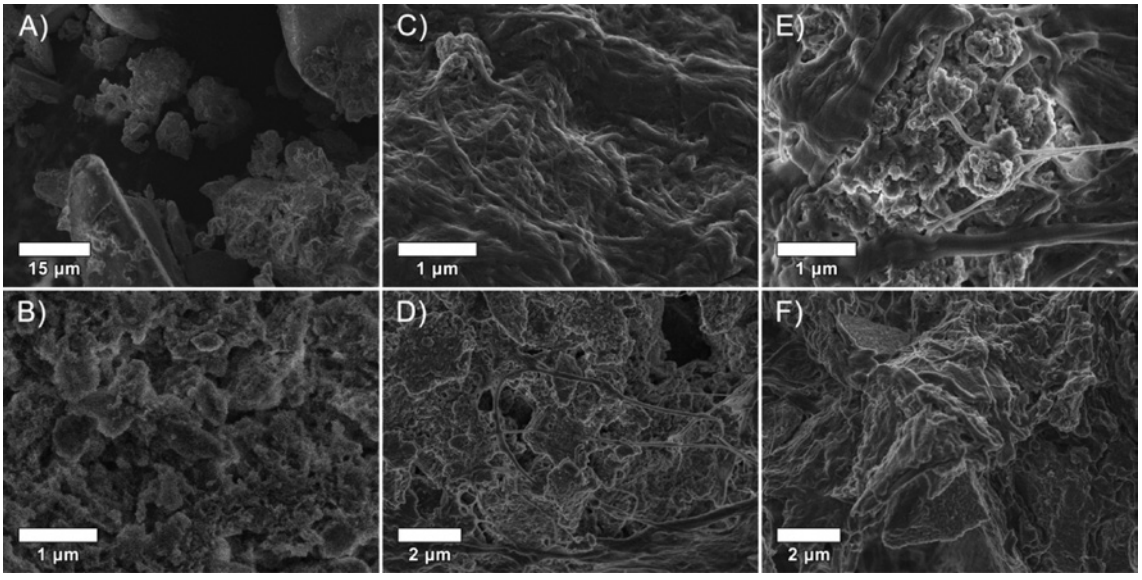

Figure 3: SEM images. Lap@Eu (A) and (B); CNF/Lap@[Eu(tta)$_n$] 2:1 surface (C) and cross-section (D); CNF/Lap@[Eu(tta)$_n$] 1:1 surface (E) and cross-section (F).

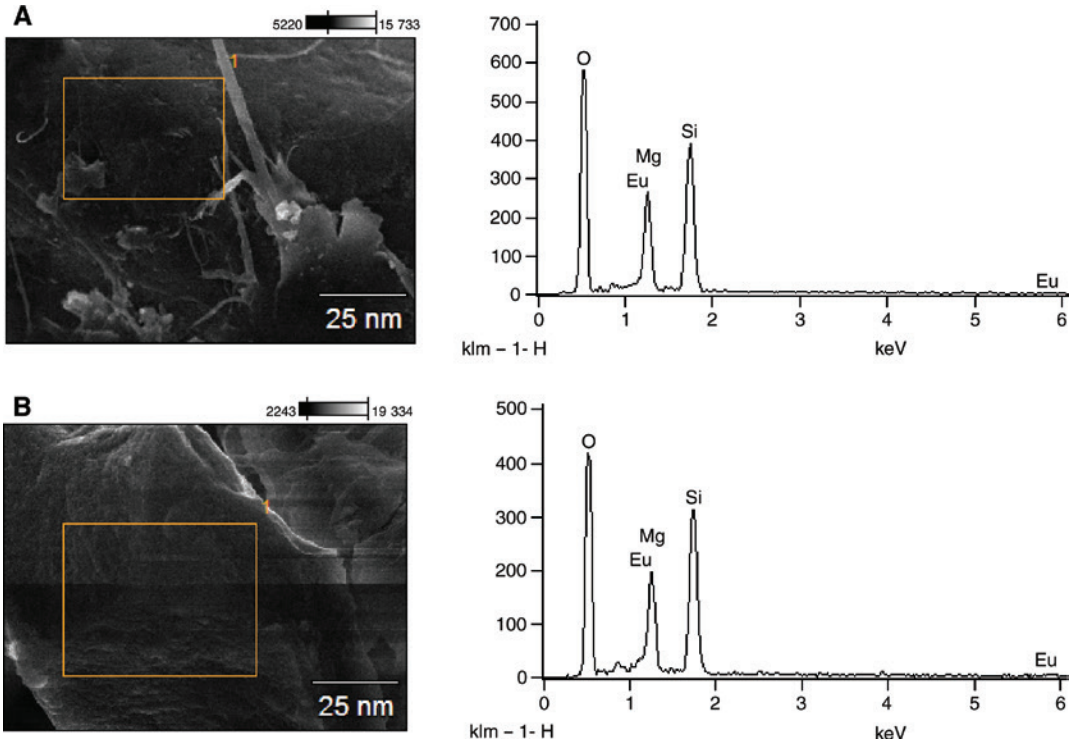

Figure 4: EDS of the films CNF/Lap@[Eu(tta)$_n$] 2:1 (A) and CNF/Lap@[Eu(tta)$_n$] 1:1 (B).

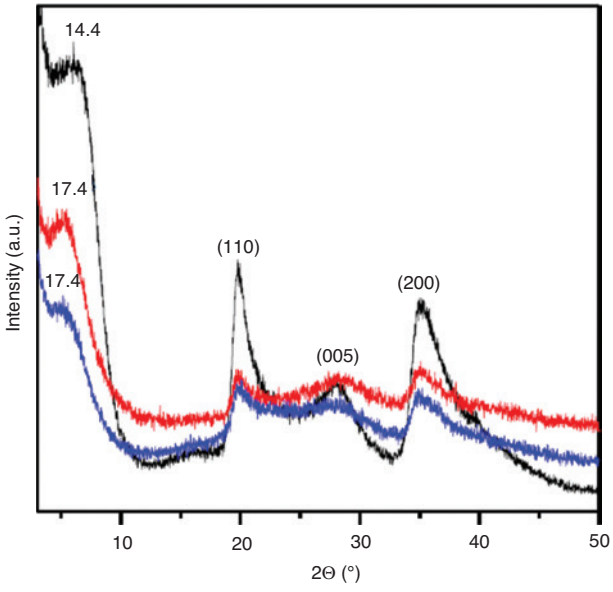

Figure 5: XRD of the sample Laponite (black), Lap@Eu (red) and Lap@[Eu(tta)n] (blue). Miller indices are indicated. d_{001}, the basal spacing referring to reflection at 6.13° of Laponite, 5.08° of Lap@Eu, and 5.09° of [Lap@Eu(tta)$_n$] is also indicated.

law [Eq. (1)] it is possible to calculate the value of the basal distance of the materials (λ = wavelength; d = basal distance; θ = diffraction angle).

$$\lambda = 2.d.\mathrm{Sen}\,\theta \quad (1)$$

Values of 14.4 Å, 17.4 Å, and 17.4 Å were obtained for Lap, Lap@Eu, and Lap@Eu(tta), respectively. An increase of 3.0 Å was observed for Lap@Eu and Lap@[Eu(tta)$_n$] compared to the pristine Laponite. The literature results show similar results. Ryu et al. [19] promoted the intercalation of Laponite with the cationic complex $[Eu(Phen)_2]^{3+}$ and observed an increase from 13.6 Å to 16.3 Å in the basal space. Yao et al. [3] reported an increase from 15.0 Å to 16.4 Å after the incorporation of the Eu^{3+}-β-diketonate complex in the basal space of the clay.

The TGA and DTG curves are presented in Figure 6. All Lap-containing materials [Lap, Lap@Eu, and Lap@Eu(tta)] present two main mass loss events. The first one (T_{onset} around 87°C, 86°C, and 79°C, with mass losses of 15.72%, 15.90%, and 13.13%, respectively) refers to water removing. The second event [T_{onset} around 726°C, 793°C, and 801°C with mass losses of 2.71%, 1.22%, and 1.21% for Laponite, Lap@Eu, and Lap@Eu(tta), respectively] is characteristic of the Laponite dehydroxylation. These mass loss events are in accord with values found in the literature [3, 5, 19]. Concerning the Lap@[Eu(tta)$_n$] hybrid, two additional mass loss events are observed. The first one with T_{onset} at 283°C (loss of 1.91%), and the second one at 434°C (loss of 1.85%), corresponding to

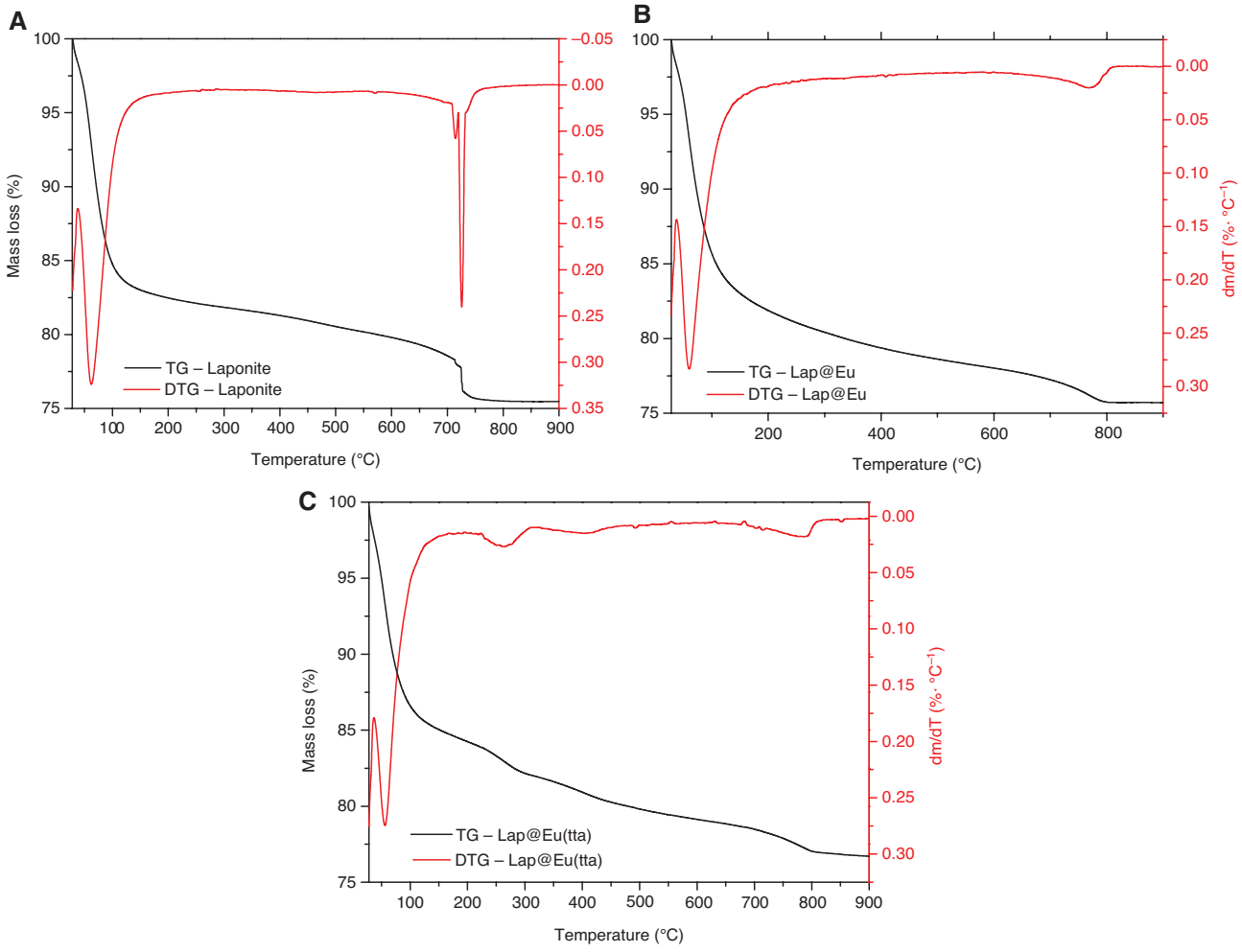

Figure 6: TGA (black) and DTG (red) curves obtained for Laponite (A), Lap@Eu (B), and [Lap@Eu(tta)$_n$] (C).

the degradation of the tta molecule at the surface and at the interlamellar space of the hybrid, respectively. In Ref. [3], a mass loss of 5% was found between 150°C and 330°C corresponding to the tta degradation. The error associated with these temperature values was estimated at 0.01%.

Figure 7 shows the results obtained for the composite films. Three mass loss events are observed, the first one appearing between 38°C and 130°C, referring to moisture removing [18, 20]. The second mass loss event, occurring between 208°C and 358°C, refers to the cellulose (and also possible existing hemicellulose residue) pyrolysis leading to volatiles and carbon. Finally, the third mass loss event occurs at different temperature ranges. For the CNF, it occurs between 370°C and 496°C (T_{onset} 445.2°C). For the sample CNF/Lap@Eu(tta) (2:1), it occurs between 370°C and 490°C (T_{onset} 469.5°C). Finally, for the CNF/Lap@Eu(tta) (1:1) sample, it occurs between 370°C and 472°C (T_{onset} 445.1°C). In the literature, events at such temperatures above 400°C are attributed to the decomposition of D-glucopyranose monomers in the form of free radicals generating residual ash [18–20].

Table 1 summarizes the results. It is clear that the presence of hybrids leads to a relative increase in the thermal stability of the cellulose counterpart. The second mass loss event is shifted to higher temperatures compared to the one observed for pristine CNF.

Figure 8 shows photoluminescence measurements. The PLE spectrum obtained for Lap@Eu shows the well-known narrow ff transitions of the $4f^6$ configuration of the Eu^{3+} ion [21–23]. The strongest one is observed at 392.8 nm ($^7F_0 \rightarrow {}^5L_6$ transition). The corresponding PL spectrum shows the characteristic transitions of the Eu^{3+} ion as well ($^5D_0 \rightarrow {}^7F_J$ J = 0, 1, 2, 3, and 4). The highest intensity was observed at 615 nm ($^5D_0 \rightarrow {}^7F_2$ transition) [21–23]. The $^5D_0$ decay curve, not shown here, could be fitted to a single exponential decay function. The lifetime value so obtained was 0.23 ± 0.01 ms.

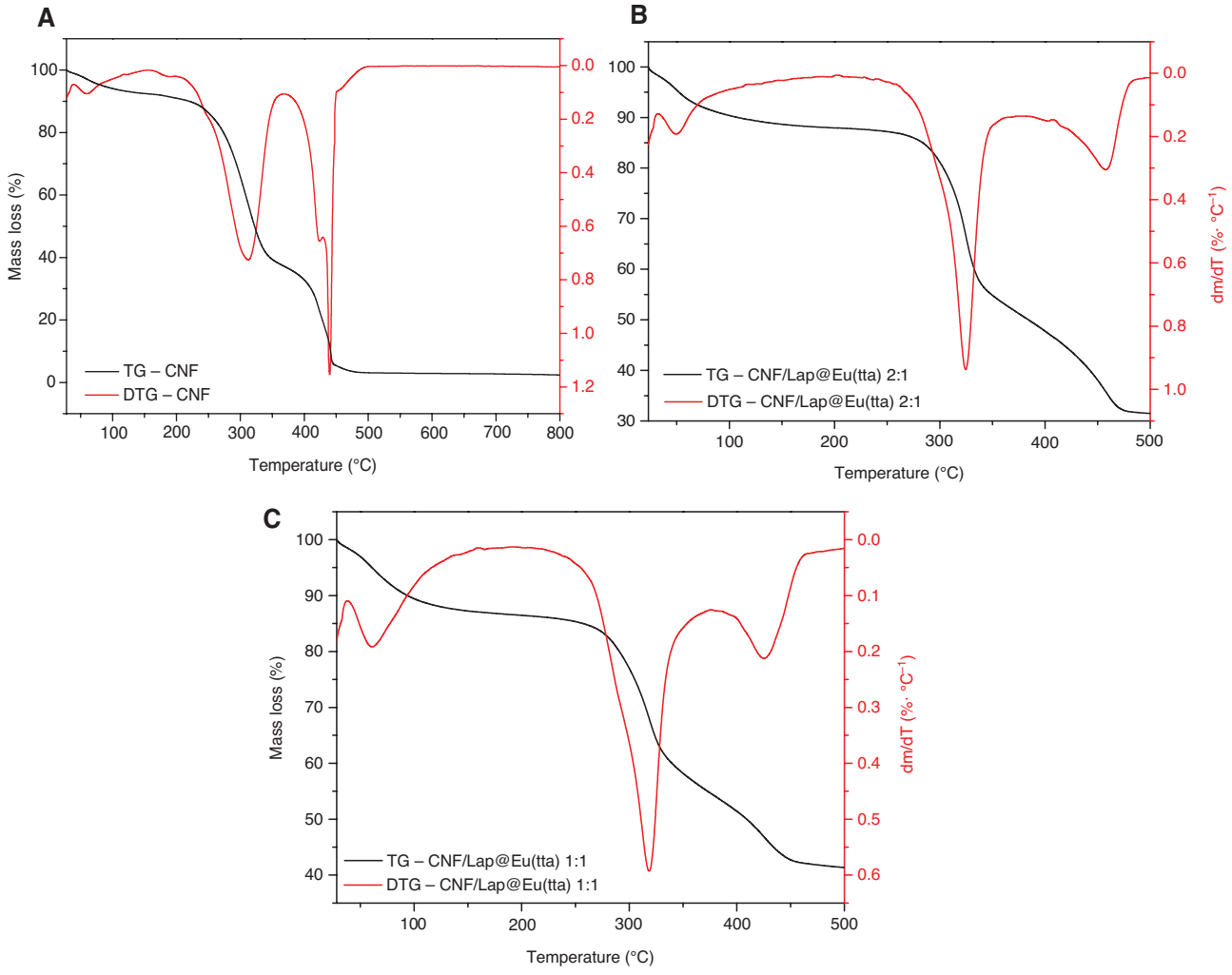

Figure 7: TG (black) and DTG (red) curves obtained for CNF (A), CNF/Lap@[Eu(tta)$_n$] 2:1 (B), and CNF/Lap@[Eu(tta)$_n$] 1:1 (C).

Table 1: Mass loss data for CNF and CNF/Lap@[Eu(tta)$_n$] 2:1 and 1:1.

Sample	38°–130°C	208°–358°C 193°–370°C (CNF)	360°–456°C 370°–496°C (CNF)	370°–472°C	370°–490°C
CNF	6% (T_{onset} = 85)	55.7% (T_{onset} = 267)	33.9% (T_{onset} = 445.2)	–	–
CNF/Lap@Eu(tta)$_n$ 2:1	8.5% (T_{onset} = 71.5)	34.4% (T_{onset} = 303.8)	–	–	20.4% (T_{onset} = 469.5)
CNF/Lap@Eu(tta)$_n$ 1:1	10.8% (T_{onset} = 89.3)	29.1% (T_{onset} = 290.4)	–	13.3% (T_{onset} = 445.1)	–

The reciprocal of the experimental lifetime (t_{Exp}) is the total decay rate (A_{total}), which brings contributions from radiative and non-radiative decays ($A_{total} = t_{Exp}^{-1} = A_{rad} + A_{n\text{-}rad}$). Interestingly enough, in the case of the Eu^{3+}, the purely radiative contribution (A_{rad}) can be obtained from the emission spectrum by taking the magnetic dipole transition $^5D_0 \rightarrow {}^7F_1$ as an internal intensity reference, according to Eq. (2) [21–23].

$$A_{0\rightarrow j} = A_{0\rightarrow 1} \cdot \frac{I(^5D_0 \rightarrow {}^7F_j)}{I(^5D_0 \rightarrow {}^7F_1)} \cdot \frac{\bar{\nu}_{0\rightarrow 1}}{\bar{\nu}_{0\rightarrow j}} \quad (2)$$

The $A_{0\rightarrow j}$, $A_{0\rightarrow 1}$ are the Einstein's spontaneous emission coefficient values for the $^5D_0 \rightarrow {}^7F_j$ and $^5D_0 \rightarrow {}^7F_1$ transitions of europium, respectively; $I(^5D_0 \rightarrow {}^7F_j)$ and $I(^5D_0 \rightarrow {}^7F_1)$ are the values of the integrated areas of the emission peaks referring to the $^5D_0 \rightarrow {}^7F_j$ and $^5D_0 \rightarrow {}^7F_1$ transitions of

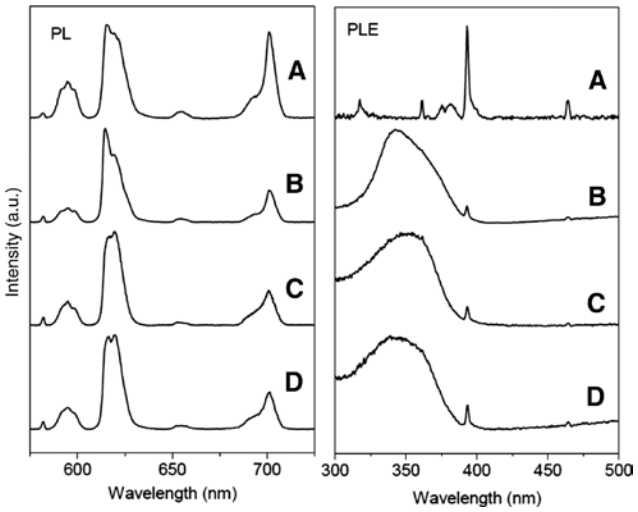

Figure 8: Photoluminescence excitation (PLE, left) and emission (PL, right) spectra. Lap@Eu (A), Lap@[Eu(tta)$_n$] (B), CNF/Lap@[Eu(tta)$_n$] 2:1 (C), and CNF/Lap@[Eu(tta)$_n$] 1:1 (D).

europium also obtained experimentally; $\bar{\nu}_{0\to1}$ and $\bar{\nu}_{0\to j}$ are the values of the barycenters of transitions $^5D_0\to{}^7F_j$ and $^5D_0\to{}^7F_1$, respectively [21–23].

A_{Rad} can be obtained with Eq. (3), and consequently, A_{NRAD} can also be obtained. The reciprocal of these quantities gives the corresponding lifetime values of τ_{RAD} and τ_{NRAD} [Eq. (4)] [21–23].

$$A_{Rad} = \sum A_{0\to j} \tag{3}$$

$$\tau_{Rad} = \frac{1}{A_{Rad}} \text{ or } \tau_{NRad} = \frac{1}{A_{NRad}} \tag{4}$$

The values so obtained are gathered in Table 2. The ratio between the experimental and radiative lifetime gives the $^5D_{0\,level}$ quantum efficiency (n), Eq. (5) [21–23].

$$n = \frac{A_{Rad}}{A_{Rad} + A_{NRad}} \tag{5}$$

Moreover, the number of water molecules (w) coordinated to the Eu^{3+} may also be estimated from the experimental and radiative decay times from the well-known Horrock's formula [Eq. (6)] [21–23]. The values are shown in Table 2.

$$w = 1.11\left(\frac{1}{\tau_{exp}} - \frac{1}{\tau_{rad}} - 0.31\right) \tag{6}$$

All pieces of information taken from photoluminescence studies contribute to the understanding of the interaction of Eu^{3+} with the Laponite layers. When compared to the spectra obtained for the precursor Eu^{3+} solution (spectra not shown here. They can be observed in Ref. [22]), completely different PL and PLE are observed. In the Eu^{3+}solution [22], Eu^{3+}ions are known to be coordinated to eight to nine water molecules [21–23]. The experimental $^5D_0$ is 0.10 ms. When introduced in the Laponite suspension (pH ~8), partial hydrolysis of Eu^{3+} occurs, followed by the interaction with Laponite hydroxide groups. These Eu^{3+} ions are, therefore, characterized by the spectra shown in Figure 8A and the data presented in Table 2. A quantum efficiency of 6.7% for $^5D_0$ and 4.2 water molecules together with OH functional groups from the Laponite layers at the first coordination sphere, complete the description of the Eu^{3+} species.

The pH8 surroundings is also important concerning the *in situ* formation of the luminescent species involving the htta ligand. In the basic pH, htta molecules are deprotonated and anionic tta ligand easily coordinates with the Eu^{3+}.

The PLE spectrum, obtained for Lap@[Eu(tta)$_n$] hybrid (Figure 8B), is dominated by a broad asymmetric UV band peaking at ~343 nm that is assigned to the $S_0\to S_1$ transition of the tta ligand [24]. Energy absorbed by the ligand is afterward transferred to Eu^{3+} leading to an enhanced emission. This is the so-called antenna effect [21–23]. The observation of this broad band in the PLE spectrum gives evidence for the formation of the Eu^{3+}-tta complex in Laponite. The emission spectrum displays bands at 582 nm, 594 nm, 614 nm, 654 nm, and 701 nm. The first visual observation is that the relative intensities observed mainly for the $^5D_0\to{}^7F_4$ transition at around

Table 2: Eu^{3+} $^5D_0$ lifetime (τ_{exp}), total decay rate ($A_{total}=1/\tau_{exp}$), radiative decay rate (A_{rad} obtained from PL spectra with Eq. 2), quantum efficiency ($n=\tau_{exp}/\tau_{rad}$ where $\tau_{rad}=1/A_{rad}$) and number of coordinated water molecules w obtained with Eq. 5.

Sample	τ_{exp} (ms) (±0.01)	A_{total} (ms^{-1})	A_{rad} (±10%) (ms^{-1})	τ_{rad} (ms)	n (%)	w
Lap@Eu	0.23	4.35	0.29	3.44	6.7	4.2
Lap@[Eu(tta)$_n$]	0.31	3.23	0.45	2.22	14.0	2.8
CNF/Lap@[Eu(tta)$_n$] 2:1	0.35	2.86	0.35	2.86	12.2	2.5
CNF/Lap@[Eu(tta)$_n$] 1:1	0.35	2.86	0.38	2.64	13.2	2.4

A_{rad} is obtained from the emission spectra, and the number of coordinated water molecules w was obtained with Eq. (5).

700 nm differ from those observed for Lap@Eu. In Lap@Eu^{3+}, the $^5D_0 \rightarrow {}^7F_4$ transition is the one with the highest intensity (Figure 8A), while in the spectrum obtained for Lap@[$Eu(tta)_n$] (Figure 8B), the $^5D_0 \rightarrow {}^7F_2$ transition is the one with the highest intensity. The $^5D_0$ lifetime in this last case is 0.31 ± 0.01 ms. Table 2 shows that the Eu-tta species formed display an enhanced $^5D_0$ quantum efficiency (n = 14.0%). The number of water molecules in the Eu^{3+} first coordination sphere is w = 2.8. We may conclude that the tta molecules substitute for water molecules coordinating with Eu^{3+}, compared to Lap@Eu.

Figure 7 and Table 2 show that the composites, formed by the introduction of the hybrids in the CNF fibers network, led to some spectroscopic changes. The broad band is still observed in the UV part of the PLE spectra. It is shifted to 358 nm. The PL spectra show small changes mainly related to relative intensities of the stark components observed at ~615 nm and ~620 nm for the $^5D_0 \rightarrow {}^7F_0$ transition. As the Eu^{3+} spectroscopic properties are very sensitive to small changes in the coordination surroundings, we may speculate at this point that the introduction of the hybrid in the CNF network leads to small changes in the coordination surroundings. Lifetime and quantum efficiency values change by less than 10% compared to those of La@[$Eu(tta)_n$]. A detailed low-temperature spectroscopic study could give new information about these changes and will be the subject of future publications.

4 Conclusions

New luminescent organic-inorganic hybrid composites were obtained using Laponite bidimensional nanocrystals as hosts to luminescent species. The *in situ* formation of Eu-tta (tta-thenoylbetadiketonate) species is shown as evidenced by the observation of increasing the typical Laponite interlayer distance. Luminescent properties were also studied in order to further characterize the nature of the interaction Laponite-Eu^{3+}. Afterward, luminescent self-supporting films were obtained using green cellulose nanofibers together with the hybrids. Films are flexible, luminescent, and bring the Laponite vehicle, which was observed to increase the thermal stability of the cellulose counterpart. The new organic-inorganic hybrids can find applications, for example, as new luminophors and luminescent sensor platforms.

Acknowledgments: Brazilian funding agencies CNPq, CAPES, and FAPESP, and the Brazilian National Institute of Photonics (INFO) are acknowledged.

References

[1] M. M. Lezhnina, T. Grewe, H. Soehr and U. Kynas, Angew. Chem. – Int. Ed. 51(42), 10652–10655 (2012).
[2] M. M. Lezhnina and U. H. Kynast, Opt. Mater. 33(1), 4–13 (2010).
[3] Y. Yao, Z. Lia and H. Li, RSC Adv. 5, 70868–70873 (2015).
[4] D. Yang, J. Wang and H. Li, Dyes Pigm. 118, 53–57 (2015).
[5] J. Tronto, S. J. L. Ribeiro, J. B. Valim and R. R. Gonçalves, Mater. Chem. Phys. 113(1), 71–77 (2009).
[6] F. Carosio, F. Cuttica, L. Medina and L. A. Berglund, ACS Appl. Mater. Interfaces 7(10), 5847–5856 (2015).
[7] M. M. Lezhnina, M. Bentlage and U. H. Kynast, Opt. Mater. 33(10), 1471–1475 (2011).
[8] H. P. S. A. Khalil, A. H. Bhat and A. F. I. Yusra, Carbohydr. Polym. 87, 963–979 (2012).
[9] Y. Zhang, T. Nypelö, C. Salas, J. Arboleda, I. C. Hoeger, et al., J. Renew. Mater. 1(3), 195–211 (2013).
[10] M. J. John and S. Thomas, Carbohydr. Polym. 71(3), 343–364 (2008).
[11] N. Saba, F. Mohammad, M. Pervaiz, M. Jawaida, O. Y. Alothman, et al., Int. J. Biol. Macromol. 97, 190–200 (2017).
[12] T. Nishino, I. Matsuda and K. Hirao, Macromolecules 37, 7683–7687 (2004).
[13] O. Nechyporchuk, M. N. Belgacem and J. Bras, Ind. Crops Prod. 93, 2–25 (2015).
[14] D. Bendahou, A. Bendahou, B. Seantier, Y. Grohens and H. Kaddami, Ind. Crops Prod. 65, 374–382 (2015).
[15] Y. Zhang, T. Nypelo, C. Salas, J. Arboleda, I. C. Hoeger, et al., J. Renew. Mater. 1(3), 195–211 (2013).
[16] T. Abitbol, A. Rivkin, Y. Cao, Y. Nevo, E. Abraham, et al., Curr. Opin. Biotechnol. 39, 76–88 (2016).
[17] H. Valo, M. Kovalainen, P. Laaksonen, M. Häkkinen, S. Auriola, et al., J. Control. Release 156(3), 390–397, (2011).
[18] G. F. Perotti, H. S. Barud, Y. Messaddeq, S. J. L. Ribeiro and V. R. L. Constantino, Polymer 52(1), 157–163 (2011).
[19] S.-J. Ryu, A. Kim, M. D. Kim, S. W. Hong, S. S. Min, et al., Appl. Clay Sci. 101, 52–59 (2014).
[20] H. S. Barud, J. M. A. Caiut, J. Dexpert-Ghys, Y. Messaddeq and S. J. L. Ribeiro, Compos. Part A Appl. Sci. Manuf. 43(6), 973–977 (2012).
[21] L. D. Carlos, R. A. S. Ferreira, V. Zéa-Bemudez and S. J. L. Ribeiro, Adv. Mater. 21(5), 509–534 (2009).
[22] F. A. Dias Filho, L. D. Carlos, Y. Messaddeq and S. J. L. Ribeiro, Langmuir 21, 1776–1783 (2005).
[23] K. Binnemans, Coord. Chem. Rev. 295, 1–45 (2015).
[24] C. Molina, K. Dahmouche, Y. Messaddeq, S. J. L. Ribeiro, M. A. P. Silva, et al., J. Lumin. 104, 93–101 (2003).